Supplementary Material

Supplementary Materials and Methods

Animals

Head surgery and electrical stimulation

In all 64 animals, the head of the animals was placed in a stereotaxic frame. In **groups 1A** (n=28), **1B** (n=8) and **2A** (n=8), a midline scalp incision was made and the skull exposed. The laser-Doppler flowmetry (LDF) probe (tip diameter 1mm, fibre separation 0.25mm) attached to a flowmeter (PeriFlux 4001, Perimed AB, Järfälla, Sweden) was affixed over a burr hole with a diameter of 1mm (4-5mm lateral to midline, 1-2mm posterior to Bregma). The epidural DC/AC-ECoG was measured with two electrodes overlying the territory of the right MCA (4-5mm lateral to midline, about 4mm and 5mm posterior to Bregma) connected to a differential amplifier (Jens Meyer, Munich, Germany). Analog-to-digital conversion was performed using a Power 1401 (Cambridge Electronic Design Limited, Cambridge, UK). Electrodes and LDF probe were fixed to the skull with dental cement (Paladur, Heraeus Kulzer GmbH, Hanau, Germany). The reference electrode was placed under the skin in the nuchal region. In **groups 1C** (n=12) and **2B** (n=8), the scalp was chemically depilated with hair removal cream (Pilca Enthaarungscreme, Sodalco, Milano, Italy). A horizontal small incision on the level of the Bregma was made in order to affix an LDF probe over a circular burr hole (4-5mm lateral to midline, 1-2mm posterior to Bregma). Two silver/silver chloride (Ag/AgCl) electrodes were stitched to the skin. The Ag/AgCl electrodes were prepared from silver wire flamed to produce spherical tips with a diameter of 0.6-0.8mm and then chlorodised. Abrasive electrode gel (Abralyt 2000, EasyCap, Herrsching, Germany) and conductive electrode cream (Synapse, Kustomer Kinetics In., Arcadia, CA, USA) were applied to set the electrode impedance to <5kΩ and to assure long-term stability of the signal with minimal DC potential drift. For electrical stimulation of SDs in **groups 2A** and **2B** (controls), a burr hole of 1mm diameter

was drilled 2mm frontal to the LDF probe and a bipolar stimulation electrode was placed on the pial surface (NE-200, 2x0.2mm insulated stainless steel wires separated by a 0.5mm shaft, Rhodes Medical Instruments, Summerland, CA, USA). Cathodal pulses (three consecutive pulses of 5mA, 100ms) (Master-8, A.M.P.I, Jerusalem, Israel) were applied. If no SD occurred, additional stimuli of 6mA were given resulting in SD in all animals. **Figure 1** shows the animal experimental set-ups of the five different groups.

Filament occlusion

The intraluminal filament occlusion is illustrated in **Figure 1**. The animals were placed supine on a plastic holder (Luckl *et al.*, 2009; Luckl *et al.*, 2012). The right common carotid artery (CCA) was carefully dissected from surrounding tissue and the right external carotid artery was ligated with a silk suture. A 0.39mm silicone coated nylon filament (Doccol Corporation, Redlands, CA, USA) was inserted through the CCA into the internal carotid artery (ICA).

Histology

After 72 hours of survival, all animals underwent cardiac perfusion fixation with saline and 4% paraformaldehyde (Sigma-Aldrich, St. Louis, MO, USA). The brains were only extracted from the skull after leaving them *in situ* over night to avoid the formation of dark neurons. The extracted brains were kept in paraformaldehyde at 4^{o}C for another 4-5 days. Thereafter, they were cryoprotected using increasing concentrations of sucrose from 15% to 30%, and the cerebellum was removed. After immersion into ice-cold isopentane for 30-40s, the brains were stored in a deep freezer at -80^{o}C.

Subsequently, 20µm coronal cryosections of the brains were serially collected at 1mm intervals. Sections were stained with haematoxylin according to the standard protocol of the Department of Experimental Neurology of the Charité – Universitätsmedizin Berlin. The stained sections were scanned (600 dpi) to determine the size of infarction using a computer

based image analyzer (Sigma Scan Pro 5.0, Systat, San Jose, USA). The size was computed by subtracting the area of the normal tissue in the hemisphere ipsilateral to the ischemic injury from the area of the contralateral hemisphere. Lesion volumes in cortex and striatum were determined by summation of the infarct areas of 10 brain slices integrated by the thickness. Another series of sections was stained with haematoxylin-eosin following the standard protocol of the Department of Experimental Neurology. In this series, a qualitative analysis was performed for signs of selective neuronal necrosis and/or apoptosis in animals without apparent infarct. To identify necrotic cells we used previously established criteria (Farber, 1982; Trump *et al.*, 1984) summarized by Garcia and colleagues (Garcia *et al.*, 1995). Using light microscopy, necrotic neurons can be identified as either red neurons (pyknosis/eosinophilia) or ghost neurons (complete loss of haematoxylinophilia). Pyknosis resulting from chromatin condensation is the most characteristic feature of apoptosis and can also be visualized on haematoxylin sections (Ulukaya *et al.*, 2011).

Statistical analysis of the animal experiments

Animal data were prospectively collected and analysed by comparing relative changes of CBF in relation to baseline (=100%) and absolute changes of AC-ECoG power (bandpass: 0.5–45Hz), integral of the AC-ECoG power, AC-scalp electroencephalography (EEG) power (bandpass: 0.5–45Hz) and DC potential (bandpass: 0–0.05Hz) using the recently published recommendations of the Co-Operative Studies on Brain Injury Depolarizations (COSBID) for human recordings (Dreier *et al.*, 2017). It was not possible to determine a zero level of CBF after death because the animals survived the monitoring period. When recordings showed a DC drift under baseline conditions drift correction was performed based on a linear regression model using the statistical software package R (r-project.org). The electrophysiological and CBF data were analysed in an un-blinded fashion using LabChart-7 software (ADInstruments, New South Wales, Australia). A meaningful blinding was not possible because both DC and

CBF traces immediately disclosed the animals' group affiliations (**Figure 1B**). By contrast, the histological analysis was performed in a blinded fashion.

We decided a priori to exclude animals in which either the physiological parameters were not within the normal range (body temperature of 37.5±0.5^{o}C, p_aO_2 of 90-130mmHg, p_aCO_2 of 35-45mmHg and arterial pH of 7.35 to 7.45) (case1) or the mean value of one of the recorded parameters was outside the range of two standard deviations from the mean of the respective group (case2), or histological sections, LDF recordings or electrophysiological recordings were either not available or insufficient for a meaningful analysis (case3). In **group 1A**, 35 surgeries were performed and 7 animals were excluded according to these rules (case1: n=1; case2: n=1; case3: n=5). In **group 1C**, 14 surgeries were performed and 2 animals were excluded (case2: n=1; case3: n=1). In **groups 1B**, **2A** and **2B** no animals were excluded.

Supplementary Results

Electrographic seizure activity following MCAO

Electrographic seizure activity was observed in 11/40 animals (28%) of **groups 1A** and **1C** but no animal of **group 1B** during filament occlusion. The first ictal epileptic event (IEE) started 42.0 (30.8, 50.3) min after filament occlusion. A median of 3 (2, 12) IEEs were observed in these animals that lasted for 38 (35, 54) s. Animals with IEEs showed significantly larger cortical and striatal infarcts (Mann-Whitney *U*-Tests, *P*=0.048 and *P*=0.039) and significantly worse neurological outcome (*P*=0.025).

Post-ischemic hyperperfusion following reperfusion after MCAO

After 90min of filament occlusion, CBF showed a hyperperfusion to 113 (101, 126) % (n=38). No correlation was found between the level of postischemic hyperperfusion and

infarct volume. After 15min of filament occlusion in **group 1B**, CBF showed a hyperperfusion to 109 (97, 145) % (n=8) which was not significantly different from the postischemic hyperperfusion after 90min of filament occlusion.

Control groups

In the two control **groups 2A** and **2B**, no filament occlusion was performed but 3 SDs were electrically triggered at the same time intervals as measured on average in **group 1A** between 1st, 2nd and 3rd SD during filament occlusion (2nd SD: 20.6±14.9min, 3rd SD: 36.0±15.8min) (**Figure 1B**). In **group 2A**, the negative DC shift of the 1st SD lasted for 111 (97, 129) s **rostrally** and 106 (78, 115) s **caudally**. It showed a negative amplitude of 2.1 (3.4, 1.6) mV **rostrally** and 4.1 (4.3, 3.2) mV **caudally**. This was followed by a positive potential of 1.9 (1.3, 2.5) mV and 0.9 (0.6, 1.4) mV, respectively. SD induced a drop in ECoG power (spreading depression), which started to recover after 154 (125, 181) s **rostrally** and 150 (143, 166) s **caudally**. Significant differences of these parameters were not found, either between **rostral** and **caudal** recording sites or between the 3 subsequent SDs in **group 2A**. Compared with the peak-to-peak amplitude of the 1st SD in **group 1A** (90min filament occlusion), the peak-to-peak amplitude of the 1st SD in **group 2A** (electrical stimulation) was significantly smaller (**rostral**: T-Test, P=0.005; **caudal**: Mann-Whitney U-Test, P=0.002, **group 1A**: n=28, **group 2A**: n=8) consistent with previous observations by Leão who compared DC recordings of SDs at the brain surface in a similar fashion between adequately perfused and ischemic tissue (Leão, 1947). By contrast, the amplitude of the 2nd SD in control **group 2A** was significantly larger than that in **group 1A** (**rostral**: T-Test, P=0.039, **group 1A**: n=22, **group 2A**: n=8; **caudal**: Mann-Whitney U-Test, P=0.004, **group 1A**: n=23, **group 2A**: n=8). Similar results were also found for the 3rd SD (P<0.001 at both electrode positions). The spreading hyperemia of the 1st SD in **groups 2A** and **2B** reached a level of 224 (198, 281) %

compared to baseline. It lasted for 152 (131, 159) s. These parameters did not differ significantly between 1st, 2nd and 3rd SD.

In animals with electrically induced SDs but no ischemia, the analysis did not reveal signs of selective neuronal damage (**groups 2A** and **2B**) (**Figure 2E** and **2F**). However, a small area of tissue necrosis was found in all animals at the epidural recording sites of the Ag/AgCl electrodes. Moreover, a small area of necrosis was found under the stainless steel stimulation electrodes in 13/16 animals of **groups 2A** and **2B** (in 2/16 animals, a small mechanical defect precluded proper assessment of this area). Furthermore, we found bilateral, extracellular, spongiotic artefacts due to tissue freezing in basal ganglia (10/64 animals), hippocampus (2/64 animals) and cortex (2/64 animals) (Rosene *et al.*, 1986).

Supplementary Figures

Supplementary Figure 1. Neuroimaging scans of patient 4 in Table 1 (cf. traces in Figure 3C). The figure shows representative MRI slices of the left cerebral hemisphere. The postoperative FLAIR and ADC images on Day 1 demonstrated a large subarachnoid blood clot, which extended from the orbital surface to the dorsocaudal margin of the Sylvian fissure. Posteriorly, an acute, cortical infarct had developed that appeared hypointense on the ADC map and hyperintense on FLAIR images (upper rows). Furthermore, an acute, lacunar infarct was evident in the left thalamus. The MRI on Day 7 revealed a new infarct in the left frontal lobe of the MCA territory. Notably, it involved the cortex at electrode 3 to 6 of the subdural electrode strip (rows 3 and 4). By contrast, the cortex at electrode 1 and 2 was not affected. The CT images in the lower row schematically illustrate the lesions in relation to the subdural electrode strip. The red-labelled region indicates the subarachnoid blood clot, the blue region signifies postoperative cerebral infarction on Day 1 and the green area shows the new infarct that was detected on Day 7.

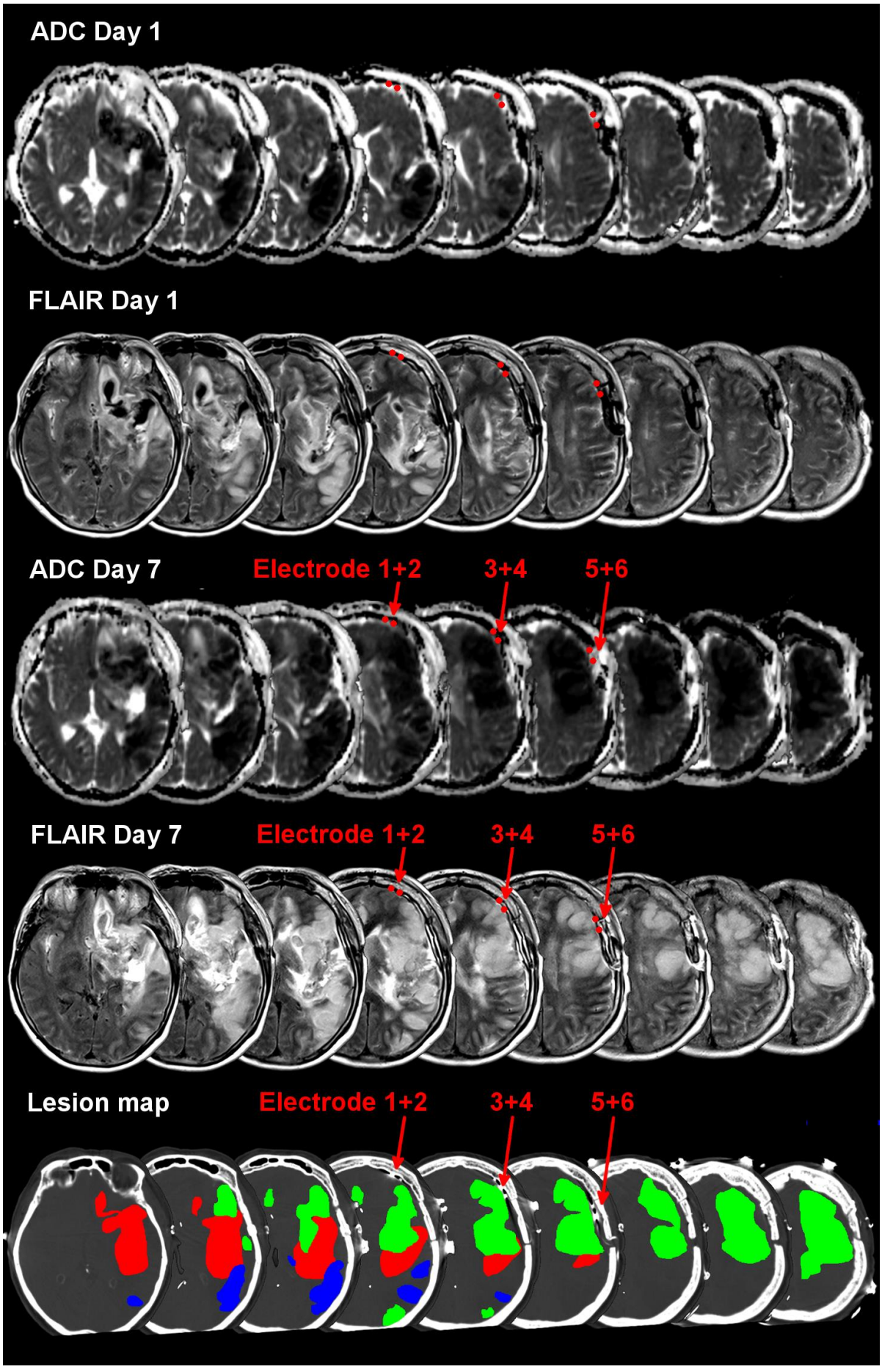
ADC Day 1
FLAIR Day 1
ADC Day 7
Electrode 1+2
3+4
5+6
FLAIR Day 7
Electrode 1+2
3+4
5+6
Lesion map
Electrode 1+2
3+4
5+6

Supplementary Figure 2. Neuroimaging scans of patient 6 in Table 1 (cf. traces in Figure 6A and B). The figure shows representative 6mm slices of two CT brain scans with a focus on the left hemisphere. The scans were performed on Day 8 and 12. The CT images on Day 8 demonstrated a subarachnoid blood clot in the left middle cranial fossa adjacent to the ruptured aneurysm. The clot was surrounded by perifocal oedema in the left, medial temporal lobe. Moreover, the whole left hemisphere appeared oedematous resulting in sulcal effacement and a midline shift of 5mm. The second CT on day 12 revealed a scattered infarct in the left MCA territory. The cortex at electrodes 4 and 6 was clearly involved in contrast to the area around electrode 1 to 3. The cortex at electrode 5 was superimposed with streak artefacts but more subtle signs of infarction are also seen below electrode 5. The lower row displays the bone window of the second CT. It illustrates the cerebral lesions in relation to the subdural electrode strip. The red-labelled area indicates the blood clot, the blue region shows the perihaematomal oedema, the green region indicates the infarct on day 12 and the red numbers signify the location of the electrodes.

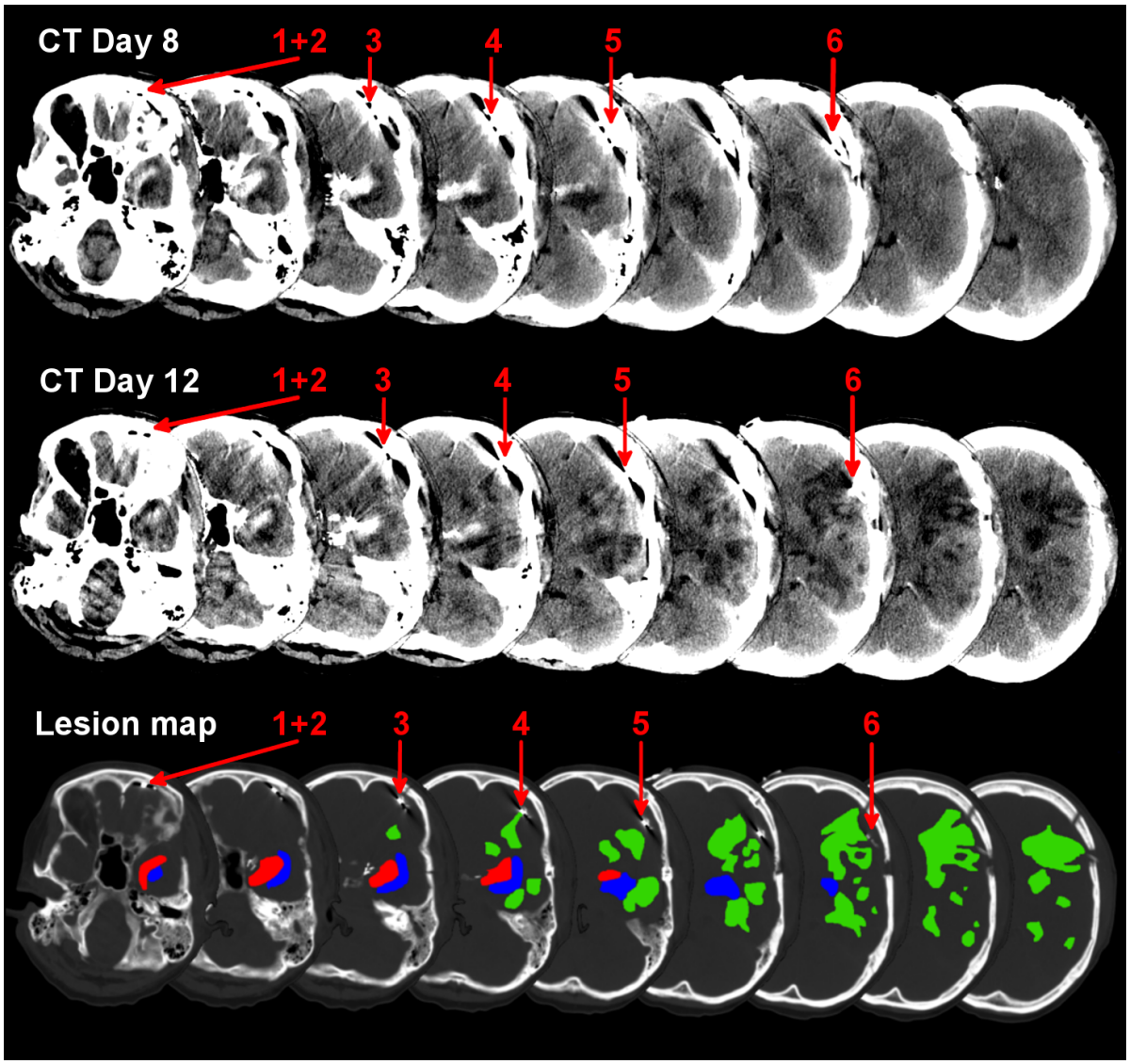
CT Day 8
1+2
3
4
5
6
CT Day 12
1+2
3
4
5
6
Lesion map
1+2
3
4
5
6

Supplementary Figure 3. Neuroimaging scans of patient 2 in Table 1 (cf. traces in Figure 6C and D). The figure shows representative MRI and CT slices of the right cerebral hemisphere. All images were aligned to the 3D T1 MPRAGE scan, which had an isometric voxel size of 1mm. Only every third slice is depicted for a better overview. DWI and FLAIR imaging on day 2 demonstrated hyperintense, cortical regions consistent with acute infarction. The lesion was predominately located in the right insular lobe. However, band-like extensions spread out from the centre to the anterior and posterior parts of the hemisphere. Posteriorly, the ascending ramus of the Sylvian fissure was involved. Anteriorly, the sulci of the inferior frontal gyrus were infarcted adjacent to electrode 6. The assessment of the cortex at the electrodes was challenging. The cortex at electrode 6 clearly appeared hyperintense on the diffusion-weighted image but the DWI signal of the gyral architecture between electrode 2 and 5 was lost, most probably due to a metallic artefact. Nevertheless, T1 MPRAGE imaging showed the gyral anatomy at the electrodes. On T1 images, the cortex was clearly hypointense typical of infarction at electrodes 4–6 in contrast to electrodes 1–3. Infarctions were additionally observed in the left posterior limb of the internal capsule and bilaterally in the cortex at the interhemispheric fissure. The CT slices in the lower row illustrate the infarct (blue-labelled area) in relationship to the subdural electrode strip. The red numbers indicate the electrodes.

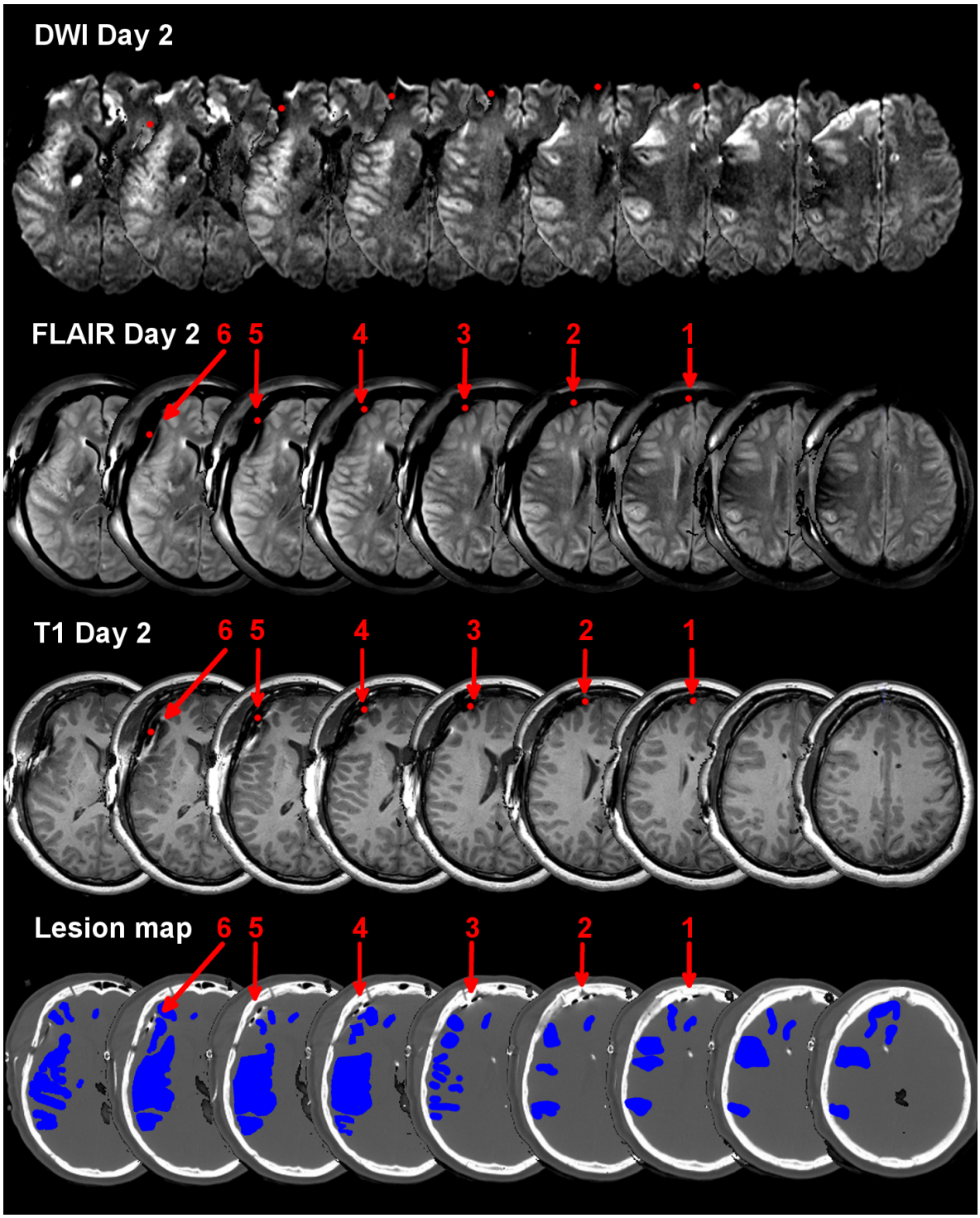
DWI Day 2
FLAIR Day 2
6
5
4
3
2
1
T1 Day 2
6
5
4
3
2
1
Lesion map
6
5
4
3
2
1

References

Dreier JP, Fabricius M, Ayata C, Sakowitz OW, William Shuttleworth C, Dohmen C, et al. Recording, analysis, and interpretation of spreading depolarizations in neurointensive care: Review and recommendations of the COSBID research group. J Cereb Blood Flow Metab 2017; 37: 1595-625.

Farber JL. Biology of disease: membrane injury and calcium homeostasis in the pathogenesis of coagulative necrosis. Lab Invest 1982; 47: 114-23.

Garcia JH, Liu KF, Ho KL. Neuronal necrosis after middle cerebral artery occlusion in Wistar rats progresses at different time intervals in the caudoputamen and the cortex. Stroke 1995; 26: 636-42; discussion 43.

Leão AAP. Further observations on the spreading depression of activity in the cerebral cortex. J Neurophysiol 1947; 10: 409-14.

Luckl J, Zhou C, Durduran T, Yodh AG, Greenberg JH. Characterization of periinfarct flow transients with laser speckle and Doppler after middle cerebral artery occlusion in the rat. J Neurosci Res 2009; 87: 1219-29.

Luckl J, Dreier JP, Szabados T, Wiesenthal D, Bari F, Greenberg JH. Peri-infarct flow transients predict outcome in rat focal brain ischemia. Neuroscience 2012; 226: 197-207.

Rosene DL, Roy NJ, Davis BJ. A cryoprotection method that facilitates cutting frozen sections of whole monkey brains for histological and histochemical processing without freezing artifact. J Histochem Cytochem 1986; 34: 1301-15.

Trump BF, Berezesky IK, Sato T, Laiho KU, Phelps PC, DeClaris N. Cell calcium, cell injury and cell death. Environ Health Perspect 1984; 57: 281-7.

Ulukaya E, Acilan C, Ari F, İkitimur E, Yilmaz Y. A Glance at the methods for detection of apoptosis qualitatively and quantitatively. Turk J Biochem 2011; 36: 261-9.

Supplementary Table 1. Changes in CBF, AC-ECoG power, scalp AC-EEG power and MAP during MCAO in rats

Variable	Groups/ number of animals			Type of test	Level of significance
		Baseline before MCAO	**Value during MCAO**		
MAP increase	**1A**, **1C**/n=40	96 (90, 107)mmHg	117 (107, 127)mmHg	Paired t-test	*P*<0.001
		Change of variable during MCAO in % of baseline (=100%)			
Rostral AC-ECoG power (first 15min)	**1A**, **1B**/n=35	35 (22, 47)%		Wilcoxon Signed Rank Test	*P*<0.001
Caudal AC-ECoG power (first 15min)	**1A**, **1B**/n=36	36 (16, 45)%		Wilcoxon Signed Rank Test	*P*<0.001
Rostral scalp AC-EEG power (first 15min)	**1C**/n=12	52 (39, 62)%		Paired t-test	*P*<0.001
Caudal scalp AC-EEG power (first 15min)	**1C**/n=12	50 (43, 61)%		Wilcoxon Signed Rank Test	*P*<0.001
CBF decrease	**1A**, **1B, 1C**/n=48	42 (27, 50)%		Paired T-Test	*P*<0.001